Exploiting a Rose Bengal-bearing, oxygen-producing nanoparticle for SDT and associated immune-mediated therapeutic effects in the treatment of pancreatic cancer.

Dean Nicholas, Heather Nesbitt, Sian Farrell, Keirin Logan, Eva McMullin, Tierna Gillan, Paul Kelly[**], Declan O'Rourke[**], Simon Porter, Keith Thomas, Barry M. G. O'Hagan, Nikolitsa Nomikou*, Bridgeen Callan, John F. Callan, Anthony P. McHale.

School of Pharmacy and Pharmaceutical Sciences, University of Ulster, Coleraine, Northern Ireland, BT52 1SA

* Department of Surgical Biotechnology, Div of Surgery & Interventional Sci., University College London, Royal Free Hospital, Pond Street, London NW3 2PF, UK

** Department of Cellular Pathology, Royal Victoria Hospital, Belfast Health and Social Care Trust, Grosvenor Road, Belfast, Northern Ireland, BT12 6BA

Authors for correspondence:

Anthony P McHale

(0044) 2870124616

ap.mchale@ulster.ac.uk

John F Callan

(0044) 2870123059

j.callan@ulster.ac.uk

Abstract

Sonodynamic therapy (SDT) is an emerging stimulus-responsive approach for the targeted treatment of solid tumours. However, its ability to generate stimulus-responsive cytotoxic reactive oxygen species (ROS), is compromised by tumour hypoxia. Here we describe a robust means of preparing a pH-sensitive polymethacrylate-coated CaO_2 nanoparticle that is capable of transiently alleviating tumour hypoxia. Systemic administration of particles to animals bearing human xenograft BxPC3 pancreatic tumours increases oxygen partial pressures (PO_2) to 20 – 50 mmHg for over 40 min. RT-qPCR analysis of expression of selected tumour marker genes in treated animals suggests that the transient production of oxygen is sufficient to elicit effects at a molecular genetic level. Using particles labelled with the near infra-red (nIR) fluorescent dye, indocyanine green, selective uptake of particles by tumours was observed. Systemic administration of particles containing Rose Bengal (RB) at concentrations of 0.1 mg/mg of particles are capable of eliciting nanoparticle-induced, SDT-mediated antitumour effects using the BxPC3 human pancreatic tumour model in immuno-compromised mice. Additionally, a potent abscopal effect was observed in off-target tumours in a syngeneic murine bilateral tumour model for pancreatic cancer and an increase in tumour cytotoxic T cells ($CD8^+$) and a decrease in immunosuppressive tumour regulatory T cells [T_{reg} ($CD4^+$, $FoxP3^+$)] was observed in both target and off-target tumours in SDT treated animals. We suggest that this approach offers significant potential in the treatment of both focal and disseminated (metastatic) pancreatic cancer.

Key Words:

SDT, oxygen, immune, abscopal, pancreatic, cancer.

1. Introduction

SDT is a stimulus-responsive approach for the treatment of solid tumours that is based on the use of a relatively harmless sonosensitiser together with ultrasound in order to elicit cytotoxic effects [1]. Targeted cytotoxicity results from ultrasound-mediated, sensitiser dependant generation of cytotoxic ROS. Although the precise mechanism by which ROS are produced in the sonodynamic process has remained unclear, recent studies by our group suggests involvement of sonoluminescence, resulting from either exogenously-added or endogenously-generated microbubbles undergoing ultrasound-induced inertial collapse and subsequent sonoluminescence-induced photoactivation of the sensitiser [2]. As a result of the tissue penetrating capabilities of ultrasound, the approach offers significant potential for the non- or minimally invasive treatment of less anatomically accessible tumours, such as pancreatic cancer.

In translating SDT to the clinic for application in the treatment of more deeply-seated lesions, two major challenges need to be addressed. Namely (i) reducing the presence of sonosensitiser in tissues between the target and the emitting surface of the extracorporeal stimulus (i.e. ultrasound) and (ii) circumventing the relatively low oxygen concentration (hypoxia) in most solid tumours in order to efficiently fuel the sonodynamic effect and production of cytotoxic ROS. In precluding the presence of sensitiser in intervening tissues, we have previously reported the design of delivery systems that use either microbubbles [3] or nanoparticles [4] to achieve site-specific deposition of the sensitisers. In the former case, site-specific deposition was achieved using ultrasound to disrupt the microbubbles as they pass through the target vasculature [3]. In the latter case, we have demonstrated that formulating the sensitiser into nanoparticles can exploit the enhanced permeability and retention (EPR) effect exhibited by many solid tumours to achieve effective sensitiser accumulation at the target site [4]. In addressing tumour hypoxia and the negative impact this may have on SDT, we have

again used both microbubble- and nanoparticle-based approaches. Using oxygen -containing microbubbles, we demonstrated for the first time that the approach can be used to enable delivery of oxygen to the tumour microenvironment (TME) to enhance SDT-based treatment of solid tumours *in vivo* [3,5]. In an alternative approach to addressing oxygen deficit, we previously reported the design of CaO_2 nanoparticles that could generate oxygen *in situ* in solid tumours [6]. When CaO_2 is exposed to water it spontaneously converts to H_2O_2 and subsequently to O_2 [Eq1]. Since the conversion is rapid, its direct use is incompatible with systemic administration. In addressing the latter, nanoparticulate CaO_2 particles were coated with a novel pH-sensitive methacrylate polymer, designed to remain intact at pH 7 and became soluble at the lower pH in the (TME) [6]. It was subsequently confirmed that the particles enabled *in situ* generation of oxygen in target tumours and, when co-administered with Rose Bengal as a photosensitiser, could be used to enhance photodynamic therapy (PDT) [6].

Here we report on a novel and robust means of preparing the pH sensitive polymer coated nanoparticles, their biodistribution in vivo and their ability to elicit fortuitous effects in tumours at the molecular genetic level. We also report on a novel CaO_2 nanoparticle in which the sonosensitiser, Rose Bengal (RB) is bound to the particle and demonstrate particle-mediated SDT effects using *in vitro* and *in vivo* pancreatic tumour models. Using a bilateral syngeneic immunocompetent murine tumour model as a target for SDT-based treatment using these RB bearing nanoparticles, we demonstrate a potent SDT-mediated abscopal effect in off-target tumours and suggest that these particles could play a significant role in SDT-mediated treatment of both focal and metastatic pancreatic cancer.

2. Materials and Methods

2.1 Reagents.

Calcium peroxide (CaO_2) (200mesh), phosphate buffered saline (PBS), methanol, ethanol, hexane, Rose Bengal (RB) and indocyanine green (ICG) were purchased from Sigma Aldrich,

UK. The BxPC3 human pancreatic adenocarcinoma cell line was obtained from the American Type Culture Collection (ATCC). The T110299 murine pancreatic adenocarcinoma cell line was a gift from Prof. Jens Siveke, (Klinikum rechts der Isar, Technical University Munich, Munich, Germany) and was isolated from primary pancreatic tumours in KPC mice (Ptfla-Cre; LSL-$Kras^{G12D}$; LSL-$Trp^{53fl/R172H}$) [7]. Matrigel® from BD Biosciences, Belgium. 6-8 week old SCID mice (C.B-17/IcrHanHsd-$Prkdc^{SCID}$) and C57BL/6JOlaHsd mice were bred in house and CD-1 mice were from Harlan, UK and animal weight ranged from 20 – 25g.

2.2 Preparation of pH-responsive, polymer-coated nanoparticles (cNPs) containing indocyanine green (ICGcNPs) or Rose Bengal (RBcNPs).

5g of CaO_2 (200 mesh) were added to 20 mL of ethanol and sonicated using an ultrasound probe for 30 min (Sonics Vibracell probe, Sonics & Materials, Newtown, CT, USA, 130 watt amplitude, 89%, 20 kHz). The suspension was centrifuged at 50 *g* for 5 min at 10°C to remove larger particulates and the supernatant was recovered. The pellet was treated in the same manner once more, supernatants from both treatment cycles were combined and centrifuged together at 454 *g* for 5 min at 10°C, yielding a turbid suspension that contained the nanoparticles. The pH-sensitive methacrylate polymer used to coat the particles was prepared as described previously [6]. To coat the particles, 20 mg of CaO_2 nanoparticles were suspended in 2 mL of ethanol containing 10mg of the dissolved polymer and dispersed by sonication in an ultrasonic bath. 3 mL of hexane was initially added under constant sonication followed by the addition of hexane dropwise over a 30-min period. The suspension was then centrifuged at 13250 *g* for 5 min to yield a pellet containing the pH-sensitive polymer-coated nanoparticles (cNPs) and this was washed with ethanol to remove any residual polymer. To prepare the RBcNPs, 3.33 mg of cNPs were suspended in a 1 mL solution of RB (1 mg/mL) in ethanol, dispersed using an ultrasonic bath. This suspension was centrifuged at 13250 *g* and the pink pellet with non-specifically bound RB was washed twice by centrifugation using ethanol. The

RB content in supernatants was determined by measuring the absorbance at 560 nm and this was used to calculate the RB content of the RBcNPs. A similar approach was used to prepare the ICGcNPs, which was also bound non-specifically to the particles. Essentially, the 1 mg/mL solution of ICG in ethanol replaced the RB solution. Both payloads were shown to be stable on the particles when stored for 24 h. Particle size was determined using dynamic light scattering (DLS) using a Malvern Zetasizer 3000HSA (Malvern, Worcs., UK) and confirmed using scanning electron microscopy (SEM) using a FEI Quanta scanning electron microscope.

2.3 Dissolved oxygen measurement

The indicated quantity of the relevant nanoparticle preparation was dispensed into degassed 10 mL of phosphate buffer (0.1 M, at either pH 6.4 or 7.4) and a Jenway 9500 DO2 meter (Cole Palmer, Staffordshire UK), calibrated according to the manufacturer's instructions was used to determine dissolved oxygen concentration (mg/L).

2.3 SDT-mediated treatment of BxPC3 cells in vitro using RBcNPs.

BxPC3 cells were maintained in RPMI-1640 medium supplemented with 10% (v/v) foetal bovine serum in a humidified 5% CO_2 atmosphere at 37 °C. Cells (5 – 6 passage) were plated in a 96 well plate at a density of 2×10^3 cells per well, incubated overnight 37 °C and treated with various concentrations of RBcNPs for 1 h in serum free medium, prior to treatment with ultrasound. Cells were exposed to ultrasound using a Sonidel SP100 sonoporator (Dublin, Ireland) for 30 s at a frequency of 1 MHz, a power density of 3 W/cm^2 ($I_{SATP;}$ spatial average, temporal peak) and a duty cycle of either 40% or 50% at a pulse repetition frequency of 100 Hz. This ultrasound power density resulted in a peak to peak acoustic pressure of 0.8 MPa in water and 0.5 MPa inside the well [8]. Contact between the bottom of the plate and the ultrasound transducer was facilitated using an ultrasound gel. After a further 2 h, the RBcNPs were removed, cells were washed with fresh medium and then incubated in serum containing

medium for a period of 24 h. Cell viability was determined using the MTT cell viability assay described previously [4].

2.4 Oxygen generation in tumours using the cNPs and analysis of expression of selected genes using RT-qPCR analysis.

All animals were treated humanely and in accordance with licensed procedures under the UK Animals (Scientific Procedures) Act 1986. The ability of the cNPs to influence tumour hypoxia was examined in the BxPC3 mouse xenograft tumour model of human pancreatic cancer. The rationale for choosing this model was that the tumours are extremely hypoxic [5]. BxPC3 cells were suspended in 50% Matrigel® and 50% phosphate buffered saline (PBS) and a 100 µL aliquot, containing 1 x 10^6 cells, was administered subcutaneously into the rear dorsum of 6-8 week old female SCID mice. Once tumours had reached an average volume of 400 mm^3 [tumour volume = width x height x length/2], animals were randomly distributed into two groups (n = 5 per group). Following induction of anaesthesia via intraperitoneal injection using Hypnorm/Hypnovel /PBS (1:1:2) and intravenous administration of cNPs (30 µL of a 20 mg/mL suspension in distilled water) via the tail vein, the oxygen partial pressure (PO_2) was recorded using an Oxylite oxygen electrode sensor every 10 s for 60 minutes. Animals were terminated and tumours excised within 1 to 2 h and RNA was extracted using a High Pure RNA Isolation kit (Roche) according to the manufacturer's instructions. 500ng quantities of RNA per tumour sample were reverse transcribed into cDNA using a First Strand cDNA synthesis kit (Roche) according to the manufacturer's instructions. cDNA from 3 tumours per group was pooled and gene expression of the target genes was analysed by RT-qPCR using a Roche RealTime Ready custom designed 96 well panel. Gene targets were based on specific genes involved in management of oxidative stress (*GPX1, 2* and *3,* and *SOD1, 2* and *3*), epidermal to mesenchymal transition (EMT)/invasion (*TWIST1, SNAI1* and *2*), hypoxia/angiogenesis (*HIF1α, ARNT and VHL, MMP9* and *VEGFA*) and cancer cell markers (*NANOG, SOX2,*

POU5F1 and *ADM*). Data were generated from two runs on the cycler and gene expression was normalised to reference genes (β-actin, *GAPDH* and *RPLPO*) and % fold change in expression was calculated.

2.5 Tumour accumulation and biodistribution of ICGcNPs

6-8 week old SCID mice were implanted with BxPC3 tumours until they had grown to an average tumour volume of 400 mm^3. Following induction of anaesthesia via intraperitoneal injection as described above, 30 μL aliquots of ICGcNP suspended in distilled water (20 mg/mL) were administered intravenously by tail-vein injection. At the indicated times mice were subjected to nIR fluorescence imaging using the ICG filter set in a Xenogen IVIS Lumina. Images were analysed using Living Image version 4.3.1. At 48 hrs mice were sacrificed and the organs were surgically harvested for immediate nIR fluorescence imaging.

2.6 SDT treatment of BxPC3 tumours in vivo using RBcNPs

BxPC3 tumours were established in 6 – 8 week old SCID mice as described above. When tumours reached an average volume of 100mm^3, animals were randomly separated into three groups (n = 3 animals per group) consisting of: (i) Control animals treated by IV administration of 30 μL of distilled water alone; (ii) animals treated with 30 μL of RBcNP (20 mg/mL, IV) in distilled water and (iii) animals treated with RBcNP (20 mg/mL, IV) plus ultrasound. Ultrasound was delivered within 5 min of administering RBcNPs using a Sonidel SP100 sonoporator (Sonidel Ltd., Dublin, Ireland) at a frequency of 1 MHz, a power density of 3 W/cm^2 ($I_{SATP;}$ spatial average, temporal peak) and a duty cycle of 30% at a pulse repetition frequency of 100 Hz for 3.5 min. Contact between the emitting surface of the ultrasound transducer and the tumour was facilitated using an ultrasound gel. All treated animals received a single treatment on Day = 0. Tumour volume and body weight were monitored throughout.

2.7 SDT treatment of a bilateral syngeneic mouse tumour model using RBcNPs

To determine if RBcNP-mediated SDT could elicit an abscopal effect at off-target tumours, a bilateral syngeneic mouse model of pancreatic cancer was established using T110299 cells [7].

Cells were maintained at 37ºC in a humidified 5% CO_2 atmosphere in high glucose DMEM with 10% FBS, 1% non-essential amino acids, 1% L-glutamine and 1% penicillin/streptomycin. Bilateral tumours were established in 6-8 week old C57BL/6JOlaHsd mice by subcutaneous injection of 5 x 10^5 cells suspended in PBS into the left and right rear dorsum. When the combined tumour volume reached an average of 100mm^3, animals were randomly separated into four groups (n = 4) consisting of (i) control untreated animals, (ii) animals treated with ultrasound alone directed at the target tumour, (iii) animals treated with RBcNPs alone and (iv) animals treated with RBcNPs plus ultrasound directed at the target tumour. 30 μL aliquots of RBcNPs in distilled water (20 mg/mL) were administered intravenously via the tail vein. Ultrasound treatment was as described above and carried out immediately after nanoparticle administration. The off-target tumour received no ultrasound. All treated animals received a single treatment on Day = 0. Tumour volume and body weight were monitored throughout.

2.8 Flow cytometry analysis

Tumours from four animals in the RBcNP plus ultrasound treatment group and four from the control untreated group were surgically removed on day 8. Tissues were homogenised in RPMI 1640 medium supplemented with 4% foetal bovine serum, 160 μL collagenase type II (30 mg/mL), 50 μL DNAse (2 μg/mL) and mixed gently for 15 min at RT. The suspension was filtered to remove clumps, washed with PBS by centrifugation at 150 g for 5 min and incubated with external antibodies exhibiting the appropriate specificities as listed in Table S1 (Thermo Scientific, UK) for 30 min in the dark. Samples were washed twice with PBS by centrifugation, fixed and permeabilised using a FIX and PERM Cell Fixation and Permeabilisation kit (Thermo Scientific, UK) according to the manufacturer's instructions. Samples were subsequently incubated with the internal antibody listed in Table S1 for 30 min at RT in the dark, washed twice with PBS by centrifugation and resuspended in flow staining buffer (BD

554657). Samples were analysed using a Beckman Coulter Gallios flow cytometer (Beckman Coulter, High Wycombe UK) and post-acquisition analysis was completed using Kaluza analysis software (Beckman Coulter, High Wycombe UK). The gating strategy employed is shown in Table 2S.

2.9 Histological analysis.

In order to determine the impact of intravenously administered nanoparticles, 24 non-tumour bearing CD-1 mice were divided into two groups, with each group consisting of equal numbers of male and female animals. Following induction of anaesthesia as described in Section 2.4, one group of animals (6 male and 6 female) received 30 µL of cNPs (20 mg/mL in distilled water) administered IV via the tail vein, while the other group (control) received a 30 µL injection of distilled water. After 7 days, animals were sacrificed and both the liver and kidneys from each animal were surgically harvested and placed in a formalin-free fixative (Accustain, Sigma Aldrich, UK). The tissues were placed in an automated tissue processor, Sakura Tissue-Tek VIP 6-E and automatically embedded on a Sakura Tissue-Tek AutoTEC a120. 5 µm sections were cut, placed on a glass slide and stained with haematoxylin and eosin (H&E) using an automated staining protocol on a Roche Ventana HE600. Additional stains (i.e. reticulin, Masson's trichrome, PASD) were used when necessary and prepared using an Automated Roche Ventana BenchMark. The stained sections were reviewed by histopathologists with expertise in liver and renal pathology, using the same protocols as outlined previously [9].

2.10 Statistical Analysis

Error was reported as ±standard error of the mean (SEM). Statistical analysis was undertaken using a GraphPad Prism. Group-wise comparisons were made using one-sided parallel group t-tests with a p-value <0.05 deemed significant.

3. Results

3.1 Nanoparticle characterisation.

In these studies, the core CaO_2 nanoparticles were generated using ultrasound-mediated physical disintegration of 200 mesh commercially available CaO_2. This approach proved to be a convenient and robust means of preparing nanoparticles with routine yields of 20 – 25%. pH-sensitive polymethacrylate coated particles (cNPs) were capable of non-specifically and stably binding significant quantities of the sensitiser RB and the nIR fluorescence imaging agent ICG (RBcNPs and ICGcNPs, respectively) with a maximum of 0.1 mg of payload bound/mg of cNPs. This represented a loading efficiency of 33%. Scanning electron microscopy analysis of the uncoated NPs, the cNPs and the ICGcNPs demonstrated that all three had diameters of less than 200 nm (Fig.1A and B).

A

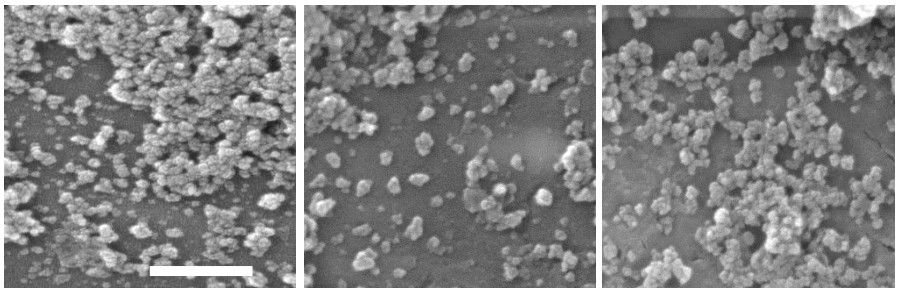

B

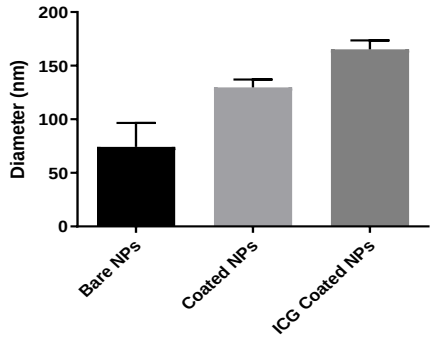

Figure 1. (A) SEM images (from left to right) of CaO_2 nanoparticles, cNPs and ICGcNPs. Size bar = 1 µm. (B) SEM derived average diameters of uncoated nanoparticles, cNPs and ICGcNPs; n = 20, where error bars represent ± SD.

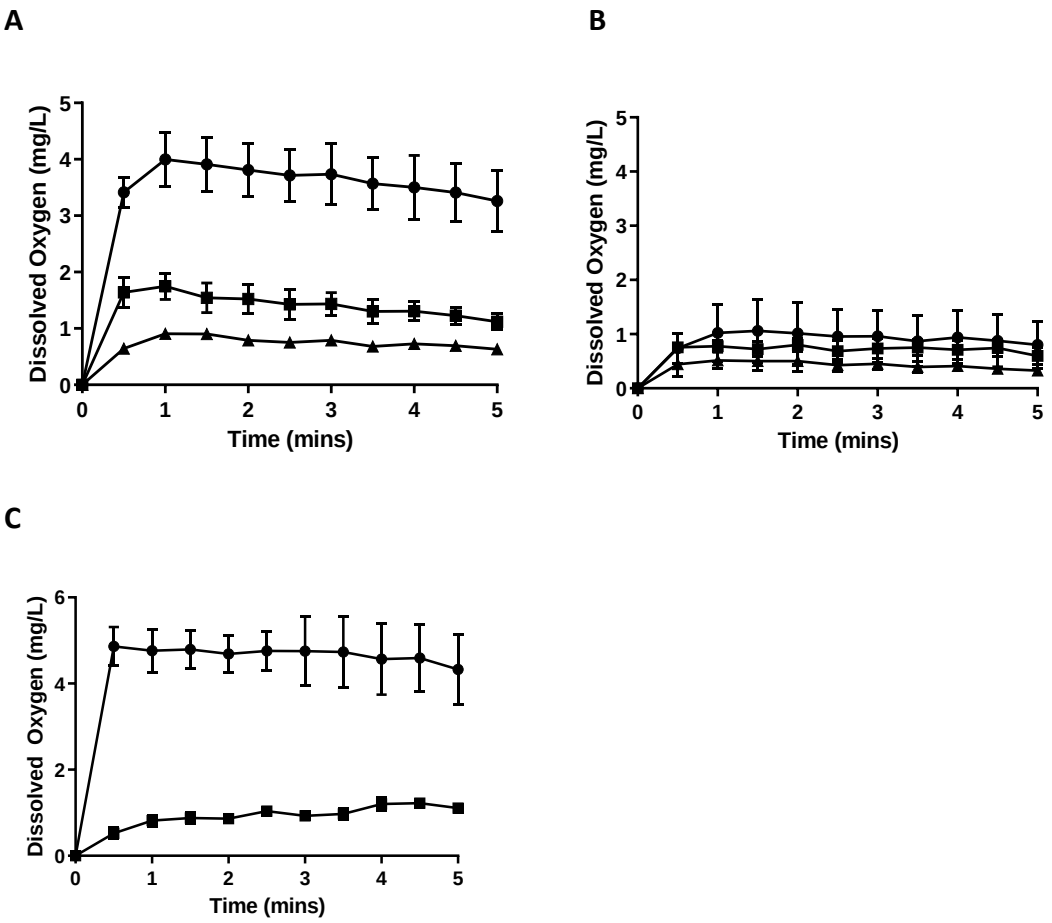

Figure 2. Oxygen generation by (A) cNPs at pH 6.4 and (B) pH 7.4 at concentrations of 0.33 mg/mL (●), 0.166 mg/mL (■) and 0.085 mg/mL (▲). (C) by RBcNPs at pH 7.4 (■) and pH 6.4 (●). Error bars represent ± SD and n = 3.

Data from DLS analyses indicated higher diameters but also demonstrated very low polydispersion indices (PDIs) with the cNPs exhibiting a hydrodynamic diameter of 246 nm and a PDI of 0.037 (Fig.S1A), whereas the RBcNPs had a hydrodynamic diameter of 280 nm and exhibited a PDI of 0.057 (Fig. S1B). Oxygen production by the cNPs at pH 6.4 and 7.4, was dose and pH dependent, producing more oxygen at pH 6.4 than at 7.4 and producing more oxygen with increasing particle dose (Fig.2A, B). Binding of RB to the cNPs had no impact on the oxygen producing response to pH (Fig.2C) and the data further demonstrate that oxygen

production at pH 6.4 occurs rapidly and reaches a maximum within the first 60 s of exposure to the low pH.

3.2 cNP-mediated oxygen generation in tumours and its impact on expression of specific tumour markers in vivo.

In order to demonstrate that cNPs were capable of oxygen generation in tumours, particles were administered intravenously to animals bearing ectopic BxPC3 tumours. The data demonstrated that the PO_2 increased within 3 min. of administering the cNPs, whereas tumours in animals that received the vehicle (distilled water) failed to exhibit any increase in oxygen partial pressure (Fig.3A). This suggested that particles were accumulating in the tumour shortly after administration. After reaching a maximum PO_2 of 54 mmHg at 3 min post injection, a steady decrease to 20 mmHg at approx. 40 min post administration was observed.

In order to determine whether or not this was sufficient to induce physiological changes, tumours were harvested between 1 and 2 h post administration of particles and analysed for expression of a broad range of specific genes associated with tumour characteristics such as management of oxidative stress, EMT/invasion, hypoxia/angiogenesis and cancer stem cell markers (Fig.3B). Analysis of expression of genes associated with the management of oxidative stress demonstrated increased expression of *GPX1*, *SOD1* and *SOD2* with downregulation of *GPX2*, *GPX3* and *SOD3*. Although no impact on *HIF1α* expression was observed, downregulation of *ARNT and VHL* did occur, suggesting an impact of oxygenation on HIF-1 function. In the context of angiogenesis, MMP9 was downregulated, although interestingly, VEGFA was upregulated. In addition, all cancer stem cell markers were downregulated as were markers for EMT/invasion and the implications of these observations will be discussed further below.

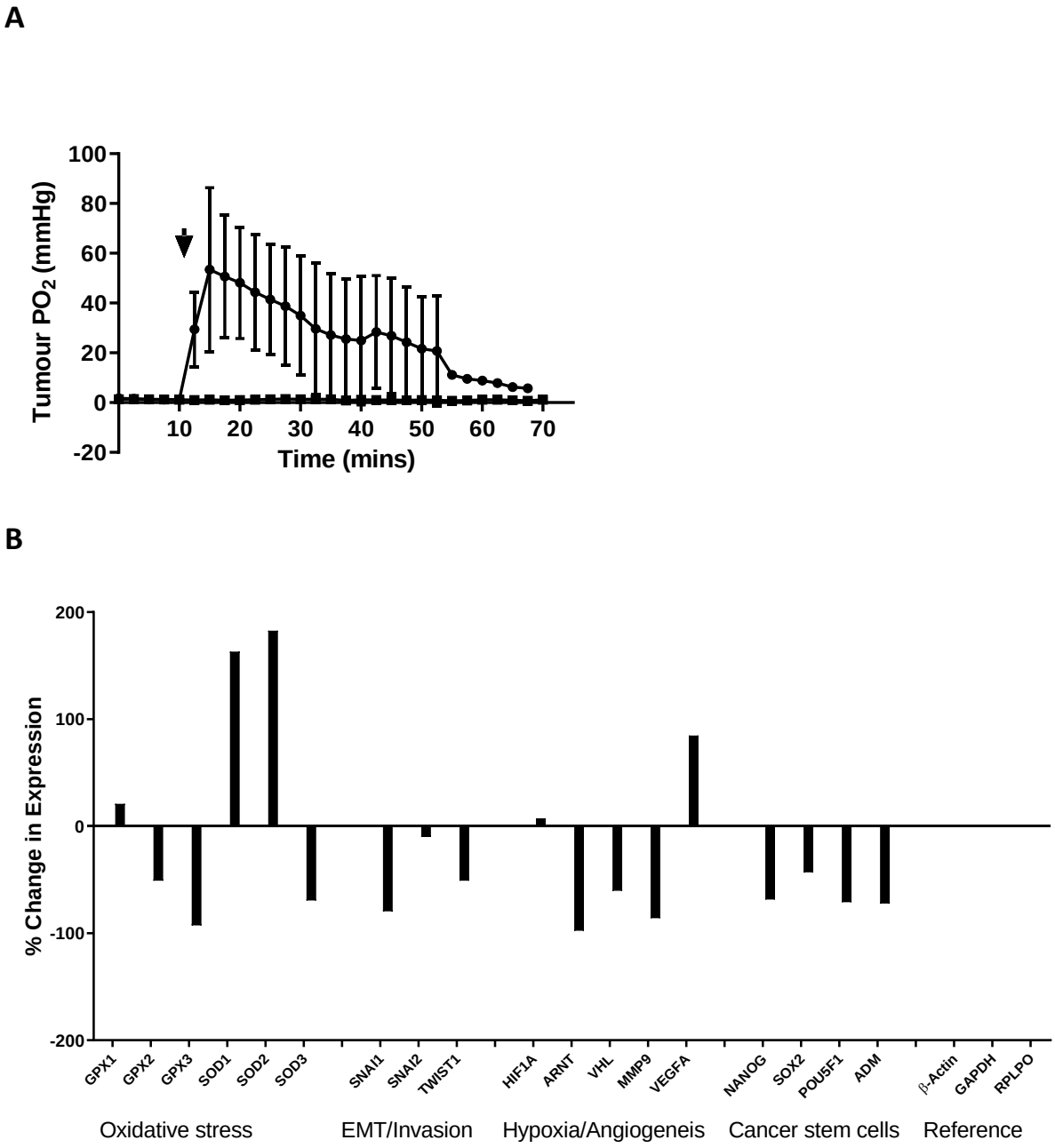

Figure 3. (A) Partial pressure of oxygen (PO_2) in BxPC3 tumours in the absence (■) and following IV administration (arrow) (●) of cNPs. Error bars represent ± SD where n = 3. (B) RT-qPCR analysis of expression of indicated genes.

3.3 Tumour accumulation and biodistribution of ICGcNPs.

Since the cNPs were capable of generating oxygen in tumours and were of a size capable of exploiting the enhanced permeability and retention (EPR) phenomenon exhibited by most solid tumours [10], it was of interest to examine particle distribution and the fate of a particle bound payload *in vivo*. To these ends, ICG was employed as a surrogate payload because it could bind to the cNPs and could be used to monitor the distribution of particles using real time nIR fluorescence imaging [4]. Following IV administration of the ICGcNPs to animals bearing BcPC3 tumours, animals were subjected to imaging over a 48 h period and the data obtained are shown in Fig.4. Although these data are semi-quantitative, the data demonstrate that a degree of tumour accumulation was evident at very early stages post administration (Fig.4A). When nIR signals from tumour tissues were expressed relative to signals received from peripheral tissues, accumulation was evident at 10 min post administration and icreased up to a period of 1 h post administration (Fig.4B, left) confirming almost immediate preferential particle accumulation in tumours. After this, the signal ratio of tumour to peripheral tissue began to decrease, although from 4 h, this again began to increase and may result from disintegration of the particles when they encountered the low pH in the TME Furthermore, when tissues were harvested 48 h post administration, it was found that tumour, liver and kidney exhibited the highest nIR fluorescence signals with lung, spleen, heart, brain and bladder providing much lower nIR signals (Fig.4C).

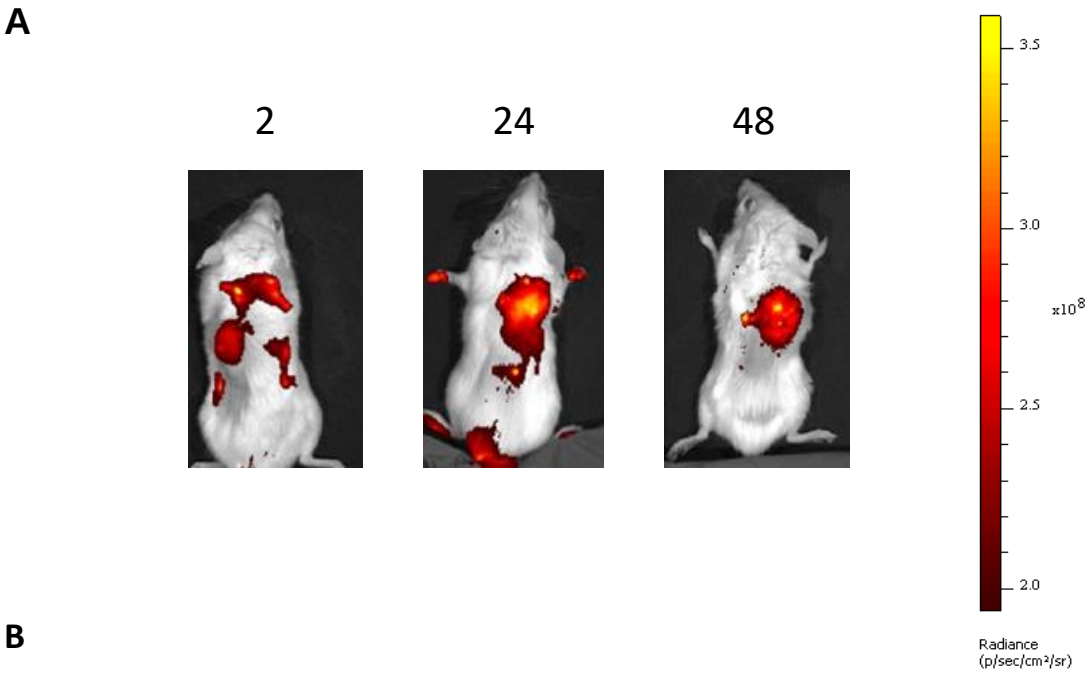

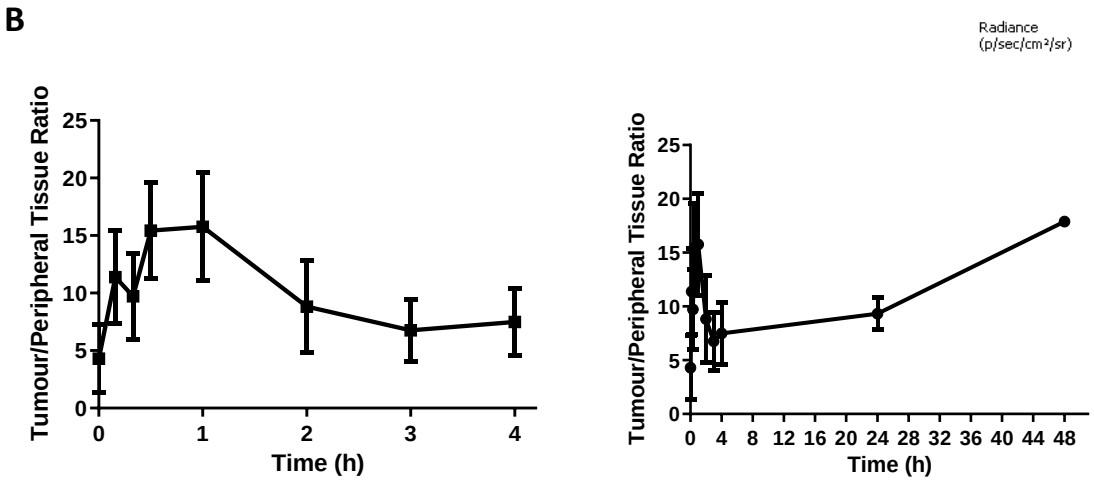

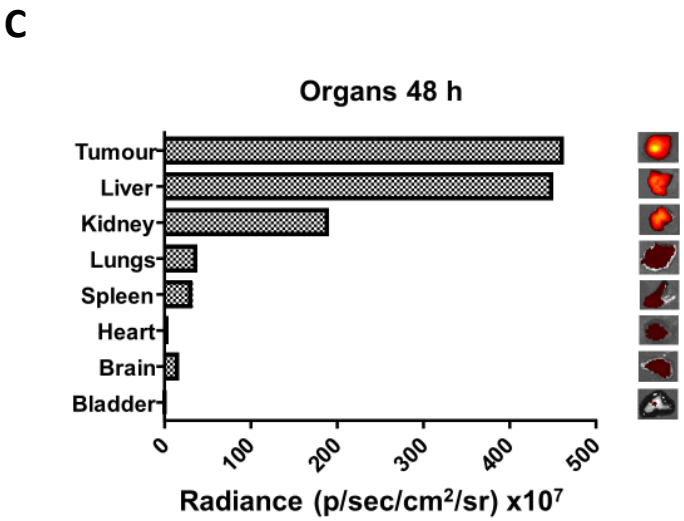

Figure 4. (A) Real time nIR fluorescence imaging of mice bearing BxPC3 tumours (arrows) following IV administration of ICGcNPs. (B) Ratio of nIR fluorescence imaging signal from

the tumour to that from peripheral tissues in animals bearing BxPC3 tumours following IV administration of ICGcNPs over short and longer time frames. Error bars represent ± SD where n = 4. (C) nIR fluorescence imaging of isolated organs 48 h after IV administration of ICGcNPs to animals bearing BxPC3 tumours.

3.4 Toxicity of systemically administered nanoparticles

In order to determine if the cNPs had any deleterious effect on either liver or kidney it was decided to examine those organs at a histological level 7 days after intravenous administration to non-tumour bearing animals. The data demonstrate that there were no significant pathological findings in either control or treated kidneys or kidneys following IV administration of cNPs (Fig.2S; Supplementary Data).

3.5 SDT-mediated treatment of BxPC3 cells **in vitro** *using RBcNPs.*

To demonstrate that the RBcNP could elicit cytotoxic effects in response to ultrasound, the human pancreatic adenocarcinoma cell line, BxPC3 was used as a target. Cells were treated with ultrasound in the presence of the RBcNPs and cell viability was subsequently determined. The data demonstrate that the particles exhibit no statistically significant effect on cell viability between concentrations of 0.1 to 0.5 µg/mL (Fig.5). At a concentration of 1 µg/mL, the particles contributed to a 40% decrease in cell viability in the absence of ultrasound. At this concentration, treatment with ultrasound at either a 40 or 50% duty cycle resulted in a decrease in cell viability to 25% and 20%, respectively (Fig.4) and these data suggest that the RBcNPs can be used to deliver an ultrasound-mediated cytotoxic effect.

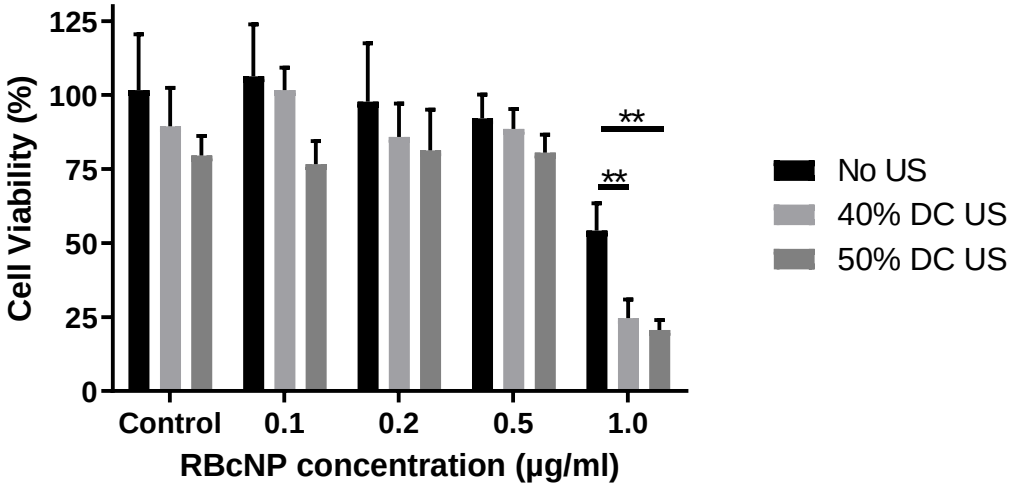

Figure 5. RBcNP-mediated SDT-based treatment of BxPC3 cells using ultrasound duty cycles of either 40% or 50% (pulse repetition rate = 100 Hz). Samples listed as No US were treated with RBcNPs. Error bars represent ± SD and n = 4. ** denotes $p<0.01$.

3.6 SDT-mediated treatment of BxPC3 tumour in vivo *using RBcNPs.*

In order to demonstrate that the RBcNPs could be employed to deliver SDT-based effects *in vivo*, a preliminary study aimed at treating ectopic xenograft BxPC3 tumours with SDT following systemic administration of RBcNPs was performed on a limited number of tumour bearing animals and the data obtained are shown in Fig.6. Some evidence of tumour growth inhibition was observed when tumours were treated with RBcNPs alone, although this was not found to be statistically significant (Fig.6A). However, treatment of tumours with RBcNPs and subsequently with ultrasound resulted in a statistically significant decrease in tumour growth even with limited animals in this preliminary study. It should also be noted that all animals failed to exhibit any overt adverse effects or observable abnormalities following exposure to the particles or particle mediated SDT and this was confirmed by maintenance of body weight throughout the experiment (Fig.6C).

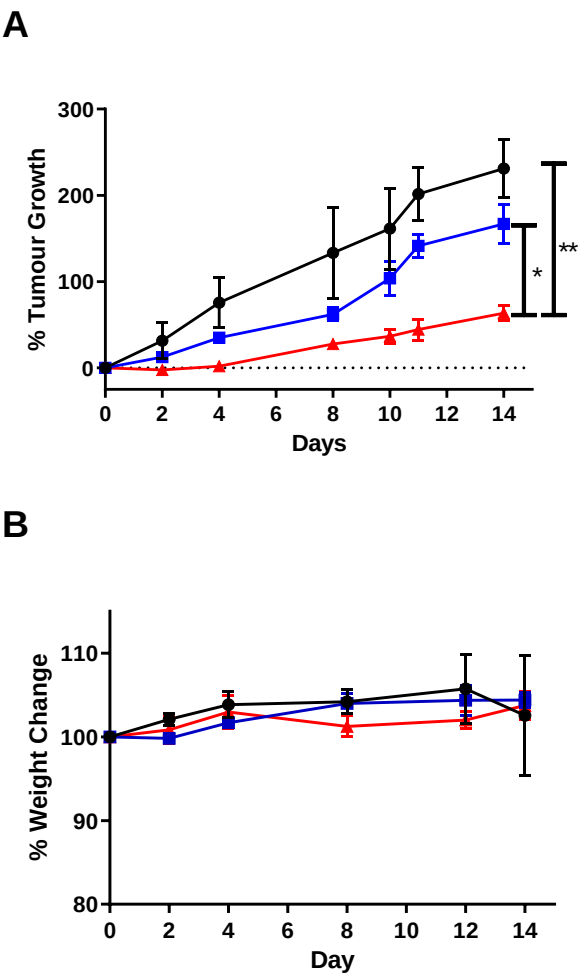

Figure 6. (A) Growth of BxPC3 tumours following treatment with vehicle (●), RBcNPs alone (■) or RBcNPs plus ultrasound (▲). (B) Animal body weight change (% starting weight) following treatment with vehicle (●), RBcNPs alone (■) or RBcNPs plus ultrasound (▲). Error bars represent ±SD n = 3 and * $p < 0.05$ and ** $p < 0.01$.

3.7 RBcNP-mediated SDT-based treatment of a murine syngeneic bilateral tumour model.

In order to determine if RBcNP-mediated SDT could elicit inhibitory effects on tumour growth at off-target tumours, a syngeneic bilateral tumour model that involved establishing a tumour on each side of the rear dorsum in each animal was used. RBcNPs were administered intravenously and only one tumour on each animal (target) was treated with ultrasound (Fig.7A). Growth of both tumours was monitored post treatment and the data obtained are

shown in Fig.7B. Control animals were either untreated, treated with RBcNPs alone or treated with ultrasound alone and no impact on tumour growth was observed in these animals. However, tumours treated with RBcNP-mediated SDT exhibited a dramatic decrease in tumour growth and it was also found that the off-target tumour in these animals that had received the particles but were not exposed to ultrasound, also exhibited a similar inhibitory effect on tumour growth.

In order to investigate this powerful abscopal effect in more detail, it was decided to harvest both target and off-target tumours from animals treated with RBcNP-mediated SDT and untreated animals on day 8 and compare tumour infiltrating immune cell populations in tumours from both groups. Using flow cytometry-based analyses, it was found that there was no statistically significant difference in the % of leucocytes ($CD45^+$) in target or off-target tumours in treated animals when compared with that in tumours from untreated control animals. Indeed, the off-target tumour actually indicating a decreasing trend (Fig.7C and D). The data did however suggest an increasing trend in the % of cytotoxic T cells ($CD8^+$) and a decreasing trend in the % of immunosuppressive regulatory T cells (T_{regs}; $CD4^+$, $Foxp3^+$) in both the target and off-target tumours when compared with those cell populations in untreated control tumours (Fig.7C and D). In addition, while the ratio of leucocytes ($CD45^+$) to immunosuppressive T_{regs} ($CD4^+$, $Foxp3^+$) indicated no statistically significant difference in tumours from treated or control untreated animals, the ratio of cytotoxic T cells ($CD8^+$) to immunosuppressive T_{regs} ($CD4^+$, $Foxp3^+$) increased significantly in both the target ($p < 0.001$) and off-target ($p < 0.05$) tumours when compared with the ratios in tumours from untreated animals (Fig.7E and F). In summary, these data suggested that RBcNP-mediated SDT can elicit an immune response that involves depletion of immunosuppressive T_{regs} together with a consequential increase in cytotoxic T cells at both the target and off-target tumours in treated animals.

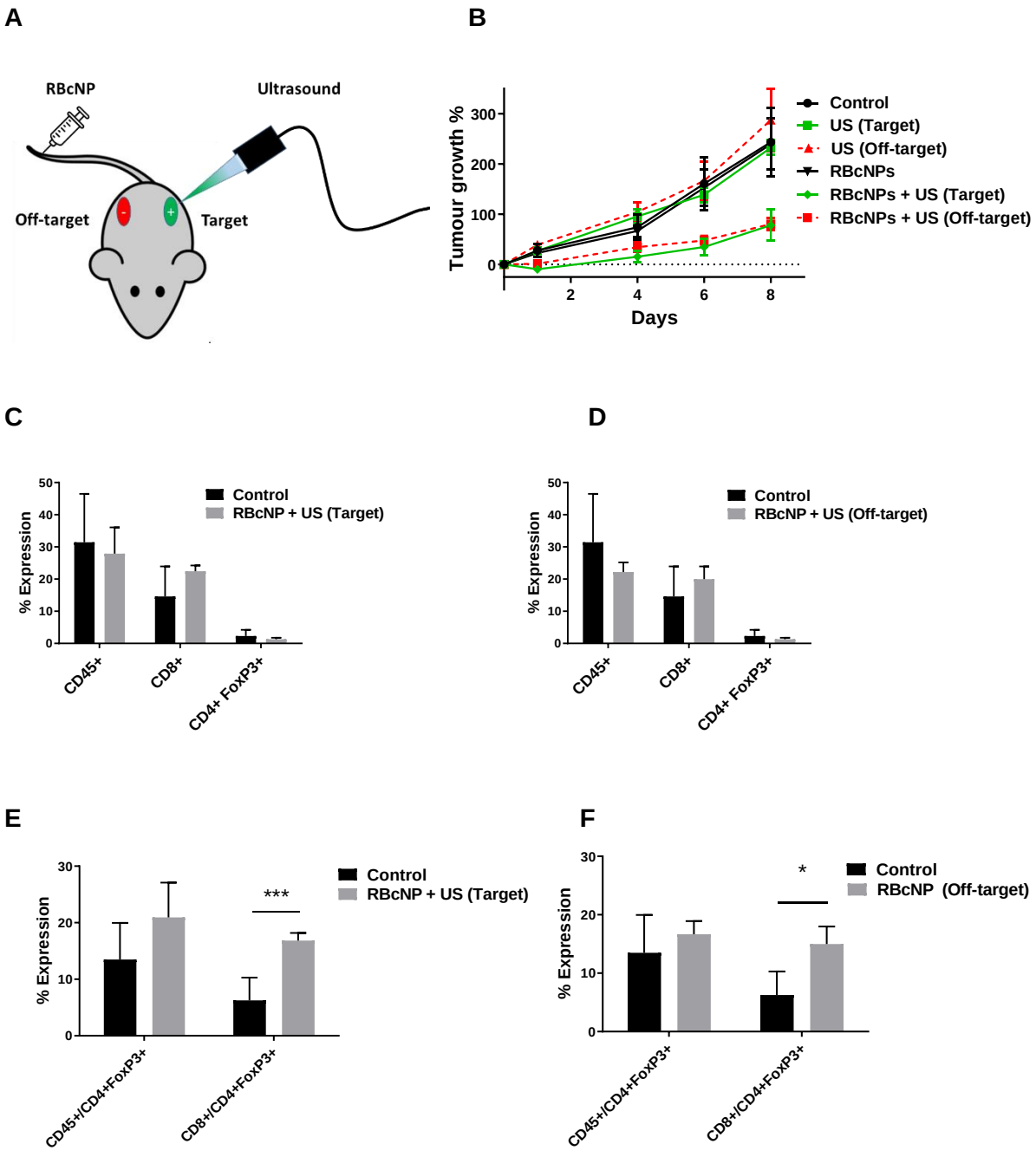

Figure 7. (A) Diagrammatic representation of the syngeneic bilateral tumour model. (B) Tumour growth over time following treatment with vehicle alone (●), ultrasound alone [target (■ solid line), off-target (▲ broken line)], RBcNPs alone [both tumours (▼ solid line)], RBcNPs plus ultrasound [target (♦ solid line), off-target (■ broken line)]. Error bars represent ± SEM where n = 4. (C & D) Comparison of tumour infiltrating leukocytes ($CD45^+$) and lymphocytes ($CD8^+$ and $CD4^+$:$FoxP3^+$) in target and off-target tumours of control animals and

those treated with RBcNP-mediated SDT. Error bars represent ± SD and n = 4. (E & F) Ratios of $CD45^+$ to $CD4^+$:$FoxP3^+$ and $CD8^+$ to $CD4^+$:$FoxP3^+$ cells in the target and off target tumours of control animals and those treated with RBcNP-mediated SDT. Error bars represent ± SD and n = 4 where * denotes $p < 0.05$ and *** denotes $p < 0.001$.

4. Discussion and conclusions

As noted above, hypoxia in the TME of solid tumours presents a significant challenge to effective SDT and this may be ameliorated by exogenous provision of oxygen. We have previously shown that CaO_2 nanoparticles facilitates *in situ* generation of oxygen in the TME of solid tumours and this can be used to enhance PDT [3]. In those studies, the nanoparticulate CaO_2 core was generated by chemical precipitation [6]. Although the method proved useful, recoveries were poor and particle aggregation during polymer coating rendered the process less efficient. However, in the current study, particles were generated by sonication in ethanol, provided good yields (20%) and were finely dispersed so that polymer coating was more efficient. Although the average hydrodynamic diameters of cNPs in the current and previous studies were similar (current = 246 nm and previous = 278 nm), the PDI of particles in the current study was extremely low, indicating more monodisperse preparations. DLS distribution data from previous studies indicated particles ranging from 100 nm to 800 nm [6] whereas in the current study particles were within the range of 200 to 500 nm. When RB was bound to cNPs the hydrodynamic diameter increased slightly to 280 nm although the PDI remained very low, indicating a very narrow size distribution (Fig.1C). This particle size was considered compatible with exploitation of the tumour EPR as shown previously with similarly sized nanoparticles [4, 10]. As noted above, the RB was non-specifically bound to the cNPs at concentrations (0.1 mg RB/mg cNP) that were compatible with SDT-based approaches as described previously [3,4,5,6] and it was further noted that no RB leaked from particles

following 24 h incubation. From a practical perspective, since it was envisaged that the particles would be employed over a short time frame post administration and since CaO_2 is inherently unstable in aqueous media, even with the polymer coating, leakage of payload was not examined over a longer period of time. The ability of the cNPs to produce oxygen in response to a decrease in pH confirmed our earlier studies, however they generated almost double the concentration of dissolved oxygen per unit mass in the current study [6]. We believe this may be the result of less aggregation of particles during the coating process in the current study.

In terms of oxygen production *in situ* in tumours, the cNPs provided tumour oxygen partial pressures (PO_2) similar to those generated in our previous study [6], reaching a maximum of over 50 mmHg 4 min after administration and sustained at over 20 mmHg for 40 min in the current study. This was significantly higher than the normal PO_2 found in BxPC3 tumours, which are known to be extremely hypoxic as confirmed in our control tumours (Fig.3A). The cNPs also provided oxygen in the tumours at physiologically relevant concentrations since the PO_2 in normal pancreatic tissues ranges from 30 – 100 mmHg [11]. In this preliminary study, RT-qPCR gene expression analysis of genes involved in key tumour processes (management of oxidative stress, metastasis/invasion, hypoxia etc,) confirmed this by demonstrating that the cNP-induced increase in oxygen had an impact on the expression of the selected gene targets in the tumour tissues exposed to the particles. One interesting finding in the study was that expression of *HIF-1α* remained relatively unchanged. In previous *in vivo* studies we have shown that provision of oxygen to the tumour microenvironment can elicit a decrease in the expression of *HIF-1α*, even 30 min after administration [12]. However, because *ARNT*, which encodes HIF-1β, was downregulated and since this is required to form the functional HIF-1 complex, the data suggested that the cNP induced oxygenation in the tumour results in inhibition HIF-1 induced transcriptional activation in the tumour [13]. In addition,

expression of *VHL* was downregulated and this was observed in previous studies describing the use of oxygenated microbubbles to enhance SDT treatment of MIA PaCa-2 pancreatic tumours in mice [9]. Another key finding in this part of the study was an increase in markers for oxidative stress such as *GPX1*, *SOD1* and *SOD2* (Fig3B). At the relatively low pH of the TME, the cNPs decompose to form H_2O_2 prior to conversion to oxygen and the former could potentially exacerbate oxidative stress that already exists in the hypoxic TME. *GPX* encodes glutathione peroxidases that scavenge H_2O_2 and of the three forms examined, only *GPX1* was elevated (Fig.3B). This suggests that the production of H_2O_2 by the cNPs is not responsible for eliciting a major anti-oxidative response, particularly since expression of *GPX2* and *GPX3* were repressed, presumably as a result of increased tumour oxygenation. Interestingly in pancreatic cancer, in addition to providing its normal function of protection against oxidative stress, *GPX1*-encoded glutathione peroxidase expression inhibits the epidermal to mesenchymal transition (EMT) by down-regulating the Akt/GSK3β/Snail signalling axis [14]. Downregulation of *SNAI1*, *SNAI2* and *TWIST1* in cNP treated tumours (Fig.3B) would seem to confirm this. The suggestion above that the initial conversion of the cNPs to H_2O_2 does not exacerbate oxidative stress is further evidenced by the upregulation of both *SOD1* and *SOD2*. Their gene products catalyse the conversion of superoxide radicals into molecular oxygen and H_2O_2 rather than responding to an increase in H_2O_2 [15]. Increased *SOD* expression would therefore represent a response to oxidative stress resulting from an acute increase in tissue molecular oxygen rather than H_2O_2. Indeed, it has been suggested that interventions designed to increase expression of *SOD1* and *SOD2* offer therapeutic potential [16]. Of the two angiogenesis markers used in these studies MMP9 was downregulated and surprisingly VEGFA was upregulated. However, it has been reported that in wound healing studies, where oxygen is provided topically, VEGFA is up regulated [17] and in the current context, the significance of this observation will require further studies with a more comprehensive panel

of gene targets. In addition to the above we also examined several markers associated with cancer stem cells, all of which were down-regulated following administration of the cNPs. Usually these cells represent less than 1 % of the number of cells in pancreatic tumours [18], but they are also the most recalcitrant to therapy and our findings could represent a fortuitous effect of administering the cNPs [19].

Clearly, the cNPs are being taken up by the tumour immediately after administration and this was confirmed at earlier stages in our imaging studies (Fig.4). However, after 1 h post administration, the degree of selectivity decreased and subsequently began to increase again. We believe that the initial decrease in selectivity may result from release of ICG into circulation with pH-mediated dissolution of the particle coat and rapid conversion of the particle core to oxygen and $Ca(OH)_2$ in the TME. The subsequent prolonged increase in the signal ratio at later stages, post administration, may result from re-uptake of the ICG by tumours. Alternatively, it could result directly from ICG on more slowly degrading particles being released in the TME that alleviates fluorescence signal quenching as a result of π-π interactions [20]. Subsequent imaging of organs at 48 h post administration confirmed that ICG was retained in the tumour, although significant fluorescent signals were also found in both liver and kidney (Fig.4). Although the above data are semi-quantitative, the payload distribution profile was remarkably like that from previous studies using PLGA-based nanoparticles of similar size [4]. These and other studies, suggested that both liver and kidney would be exposed to high concentrations of nanoparticles following systemic administration. Histological analysis of liver and kidney tissues harvested from non-tumour bearing animals exposed to the cNPs at a dose of 20 mg/kg in the current study, clearly demonstrated that the particles were non-toxic to those organs (Fig1S). The non-toxic nature of systemically administered CaO_2 nanoparticles is further supported by a recent study describing the

intravenous administration of hyaluronic acid coated CaO_2 nanoparticles at doses up to 110 mg/kg in a murine model [21].

Here we demonstrate that the RBcNP can elicit SDT-based treatments both *in vitro* and *in vivo* (Figs 5 and 6). Interestingly, tumours in animals treated with the RBcNP particles alone in the absence of ultrasound exhibited a decrease in tumour growth (Fig.6A). We have previously demonstrated that treatment with even higher doses of RB attached to microbubbles had no significant effect on tumour growth in the absence of ultrasound, using this tumour model [3]. Numerous studies in our laboratory have also demonstrated that treatment with ultrasound alone using the conditions employed in the current studies has no impact on tumour growth using this tumour model. In previous PDT-based studies, treatment with the pH-sensitive, polymer-coated CaO_2 nanoparticles in the absence of stimulus (i.e. light), had a similar effect on tumour growth using the MIA PaCa human xenograft pancreatic cancer model [6]. This effect of RBcNPs in the absence of ultrasound may result from increased oxidative stress as a result of acute exposure to molecular O_2 and downregulation of some genes involved in tumour pro-survival pathways which could negatively impact tumour growth and development, e.g. increased expression of *SOD1* and *SOD2* as discussed above [16]. Zhang *et al.* [21] reported a decrease in growth of tumours in a murine breast cancer model using hyaluronidate-modified CaO_2 nanoparticles and suggested that this was due, primarily, to the effects of increased intratumoural Ca^{2+}. The authors suggested that this may be due to an overload of Ca^{2+} in the TME which resulted in cytotoxicity. It should be noted however, that in those studies higher concentrations of CaO_2 nanoparticles (55 mg/kg) were administered, whereas we employed a dose of 20 mg/kg. The apparent benefit therefore in our stimulus-responsive approach is that lower doses of RBcNPs may be used to elicit ultrasound induced cytotoxicity in a site-specific manner. From a SDT mechanistic perspective we have previously demonstrated the production of singlet oxygen following exposure of RB to

ultrasound at conditions that are similar to those employed here [5]. This would suggest that the ultrasound conditions employed in the current study are capable of generating cavitation-based events that result in activation of the RB that, in turn, leads to the generation of reactive oxygen species such as singlet oxygen.

It has been suggested that stimulus-responsive therapies such as PDT may be capable of generating damage associated molecular patterns (DAMPs) that could, in turn, be recognised and exploited by the immune system to eradicate metastatic disease [22]. One mechanism by which this may be accomplished by PDT involves depletion of immunosuppressive regulatory T cells (T_{regs}; CD^{4+} $FoxP3^{+}$) in the TME [22]. Clearly in the current study, using the syngeneic bilateral ectopic pancreatic tumour model, RBcNP-mediated SDT induced an abscopal effect at the off-target tumour that was as effective as the SDT induced effect at the ultrasound-treated target tumour (Fig.7B). Treatment of tumours using this syngeneic model of pancreatic cancer with the RBcNPs alone had no discernible effect on tumour growth in contrast to effects observed with the xenograft model described above and reasons for this remain to be seen. Nevertheless, although there was no net increase in tumour infiltrating T cells in either the target or off-target tumours, the data suggested that the abscopal effect was due, at least in part, to a subtle decrease in tumour immunosuppressive T_{regs} (CD^{4+} $FoxP3^{+}$) and an increase in cytotoxic T cells ($CD8^{+}$) (Figs. 7 C, D, E and F) in both the target and off-target tumours. Interestingly, a study using hematoporphyrin derivative (HPD) mediated SDT [23] reported a similar abscopal effect in a murine syngeneic bilateral hepatocarcinoma model. Using immunohistochemical staining they demonstrated decreased expression of FoxP3 and increased expression of CD4 and CD8. Similarly, Yue *et al.*, [24] demonstrated a porphyrin-based, SDT-mediated abscopal effect when treating 4T1 breast tumours in mice and similar T cell distributions in both the target and off-target tumours. It should however be noted that in that study the T cell distribution in tumours resulted from immunoadjuvant and immune

checkpoint inhibitor mediated potentiation. Although the immunological studies performed in the current work are preliminary in nature, it should be noted that both hypoxia [25] and decreased pH [26] in the TME can contribute significantly to immune suppression. It remains to be seen if the transient increase in tumour oxygen or a potential increase in pH as consequence of $Ca(OH)_2$ generation following decomposition of the RBcNP, contribute to an enhanced immune effect. Regardless of the precise mechanism involved, we conclude from our studies that RBcNP-mediated SDT can deliver a potent abscopal effect that could potentially be exploited in the treatment of metastatic disease.

Acknowledgements

This authors gratefully acknowledge funding for this work under the Proof of Concept programme administered by InvestNI, Northern Ireland. Both Sian Farrell and Tierna Gillan were in receipt of postgraduate research scholarship awards from the Dept. for the Economy, Northern Ireland.

Data Availability

The raw/processed data required to reproduce these findings will be provided on request.

References

1. D. Costley, C. McEwan, C.Fowley, A.P .McHale, J. Atchison, N. Nomikou and J.F. Callan, Treating cancer with sonodynamic therapy: a review. Int. J. Hyperthermia, 31 (2015) 107-117.

2. E. Beguin, S.Shrivastava, N.V. Dezhkunov, A.P.McHale, J.F. Callan and E. Stride, Direct evidence of multibubble sonoluminescence using therapeutic ultrasound and microbubbles. ACS Appl. Mater Interfaces., 11 (2019) 19913-19919.

3. C. McEwan, S. Kamila, J. Owen, H. Nesbitt, B. Callan, M. Borden, N. Nomikou, R.A. Hamoudi, M.A. Taylor, E. Stride, A.P. McHale and J.F. Callan, Combined sonodynamic and antimetabolite therapy for improved treatment of pancreatic cancer using oxygen loaded microbubbles as a delivery vehicle. Biomaterials, 80 (2016) 20-32.

4. N. Nomikou, K. Curtis, C. McEwan, B.M.G. O'Hagan, B.Callan, J.F. Callan and A.P. McHale. A stimulus-responsive nanoparticle-based platform for use in both sonodynamic and photodynamic cancer therapy, Acta. Biomater., 49 (2017) 414-421.

5. C. McEwan, J. Owen, E. Stride, C. Fowley, H. Nesbitt, D.Cochrane, C.C. Coussios, M. Borden, N. Nomikou, A.P. McHale and J.F. Callan, Oxygen carrying microbubbles for enhanced sonodynamic therapy of hypoxic tumours. J. Control. Release, 10 (2015) 51-56.

6. Y. Sheng, H. Nesbitt, B. Callan, M.A. Taylor, M. Love, A.P. McHale and J.F. Callan, Oxygen generating nanoparticles for improved photodynamic therapy of hypoxic tumours. J. Control. Release, 264 (2017) 333-340.

7. P. Duewell, E. Beller, S.V. Kirchleitner, T. Adunka, H. Bourhis, J.Siveke, D. Mayr, S. Kobold, S. Enders and M. Schnurr, Targeted activation of melanoma differentiation-associated protein 5 (MDA5) for immunotherapy of pancreatic carcinoma. Oncoimmunology, 4 (2015) e1029698. https://doi.org/10.1080/2162402X.2015.1029698

8. E. Beguin, M.D. Gray, K.A. Logan, H. Nesbitt, Y. Sheng, S.Kamila, L.C. Barnsley, A.P. McHale, J.F. Callan and E. Stride, Magnetic microbubble mediated chemo-sonodynamic therapy using a combined magnetic-acoustic device. J. Control. Release, 317 (2020) 23-33.

9. H. Nesbitt, Y. Sheng, S. Kamila, K. Logan, K. Thomas, B. Callan, M.A. Taylor, M. Love, D. O'Rourke, P. Kelly, E. Beguin, E. Stride, A.P. McHale, J.F. Callan, Gemcitabine loaded microbubbles for targeted chemo-sonodynamic therapy of pancreatic cancer. J. Control. Release, 279 (2018) 8 – 16.

10. J. Park, Y. Choi, H. Chang, W. Um, J.H. Ryu and I.C. Kwon. Alliance with EPR effect: Combined strategies to improve the EPR effect in the tumor microenvironment, Theranostics, 9 (2019) 8073-8090.

11. H. Komatsu, C. Cook, C.H. Wang, L. Medrano, H. Lin, F. Kandeel, Y.C. Tai and Y. Mullen, Oxygen environment and islet size are the primary factors of isolated pancreatic islet survival. PLoS ONE, 12 (2017) e0183780, doi: 10.1371/journal.pone.0183780

12. J. Owen, C. McEwan, H. Nesbitt, P. Bovornchutichai, R. Averre, M. Borden, A.P. McHale, J.F. Callan, E. Stride. Reducing tumour hypoxia via oral administration of oxygen nanobubbles. PLoS One, 11 (2016) e0168088, doi: 10.1371/journal.pone.0168088

13. L. Iommarini, A.M. Porcelli, G. Gasparre and I. Kurelac, Non-canonical mechanisms regulating hypoxia-inducible factor 1 alpha in cancer. Front. Oncol. 286 (2017) doi: 10.3389/fonc.2017.00286

14. Q. Meng, S. Shi, C. Liang, D. Loang, J. Hua, B. Zhang, J. Xu and X. Yu, Abrogation of glutathione peroxidase-1 drives EMT and chemoresistance in pancreatic cancer by activating ROS-mediated Akt/GSK3β/Snai1 signalling, Oncogene., 37 (2018) 5843-5857.

15. S-H. Kim, S-H. Kim, J-H. Lee, B-H. Lee, H.J. Yoon, D.H. Shin, S.S. Park, S.B. Jang, J-S. Park and Y-K. Jee, Superoxide dismutase gene (SOD1, SOD2, SOD3) polymorphisms and antituberculosis drug induced hepatitis, Allergy Asthma Immunol. Res. 7 (2015) 88-91.

16. J.G. Wilkes, M.S. Alexander and J.J. Cullen, Superoxide dismutases in pancreatic cancer, Antioxidants 66 (2017) doi: 10.3390/antiox6030066

17. G.M. Gordillo, S. Roy, S. Khanna, R. Schlanger, S. Khandelwal, G. Phillips and C.K. Sen, Topical oxygen therapy induces vascular endothelial growth factor expression and improves closure of clinically presented chronic wounds, Clin. Exp. Pharmacol. Physiol., 35 (2008) 957-64.

18. E. Dalla Pozza, I. Dando, G. Biodani, C. Biondani, J. Brandi, C. Costanzo, E. Zoratti, M. Fassan, F. Boschi, D. Melisis, D. Cecconi, M.T. Scupoli, A. Scarpa and M. Palmieri, Pancreatic ductal adenocarcinoma cell lines display a plastic ability to bi-directionally convert into cancer stem cells, Int. J. Oncol. 46 (2015) 1099-1108.

19. C. Tang, B.T. Ang and S. Pervaiz, Cancer stem cell: target for anti-cancer therapy, FASEB, 21 (2007) 3777-3785.

20. S.P. Tarassoli, A.M. de Pinillos Bayona, H. Pye, C.A. Mossue, J.F. Callon, A. MacRobert, A.P. McHale and N. Nomikou. Cathepsin B-degradable, NIR-responsive nanoparticulate platform for target-specific cancer therapy, Nanotechnology, 28 (2017) 055101. doi: 10.1088/1361-6528/28/5/055101

21. M. Zhang, R. Song, Y. Liu, Z. Yi, X. Meng, J. Zhang, Z. Tang, Z. Yao, Y. Liu, X. Liu and W. Bu, Calcium-overload-mediated tumor therapy by calcium peroxide nanoparticles, Chem., 5 (2019) 2171-2182.

22. F. Anzengruber, P. Avci, L.F. de Freitas and M.R. Hamblin, T-cell mediated anti-tumor immunity after photodynamic therapy: why does it not always work and how can we improve it? Photochem. Photobiol. Sci., 14 (2015) 1492-1509.

23. Q. Zhang, C. Bao, X. Cai, L. Jin, L. Jun, Y. Lang, L. Li, Sonodynamic therapy-assisted immunotherapy: A novel modality for cancer treatment, Cancer Sci., 109 (2018) 1330-1345.

24. W. Yue, L. Chen, L. Yu, B. Zhou, H. Yin, W. Ren, C. Liu, L. Gao, Y. Zhang, L. Sun, K. Zhang, H. Xu and Y. Chen, Checkpoint blockade and nanosensitizer-augmented noninvasive sonodynamic therapy combination reduces tumour growth and metastases in mice. Nat. Commun. 10, 2025, doi: 10.1038/s41467-019-09760-3

25. M.Z. Noman, M. Hasmim, Y. Messai, S. Terry, C. Kieda, B. Janji and S. Chouaib, Hypoxia: a key player in antitumour immune response. A review in the theme: cellular responses to hypoxia, Am. J. Physiol. Cell. Physiol., 309 (2015) C569-C579.

26. O. Kuckuk, A. Tuccitto, D. Citterio, V. Huber, C. Camisaschi, M. Milone, B. Vergani, A. Villa, M.R. Alison, S. Carradori, C.T. Supuran, L. Rivoltini, C. Castelli and V. Mazzaferro, pH regulators to target the tumor immune microenvironment in human hepatocellular carcinoma, Oncoimmunology, 7 (2018) doi: 10.1080/2162402X.2018.1445452.

Supplementary Information

A

		Size (d.nm...	% Intensity:	St Dev (d.n...
Z-Average (d.nm): 246.6	Peak 1:	259.4	100.0	60.04
PdI: 0.037	Peak 2:	0.000	0.0	0.000
Intercept: 0.952	Peak 3:	0.000	0.0	0.000
Result quality Good				

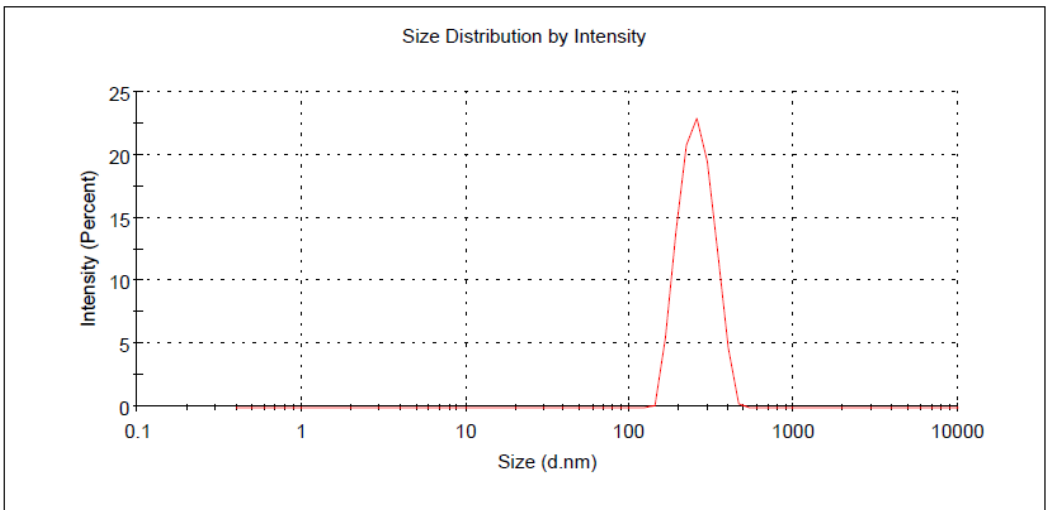

B

		Size (d.nm...	% Intensity:	St Dev (d.n...
Z-Average (d.nm): 280.4	Peak 1:	294.5	100.0	61.19
PdI: 0.057	Peak 2:	0.000	0.0	0.000
Intercept: 0.944	Peak 3:	0.000	0.0	0.000
Result quality Good				

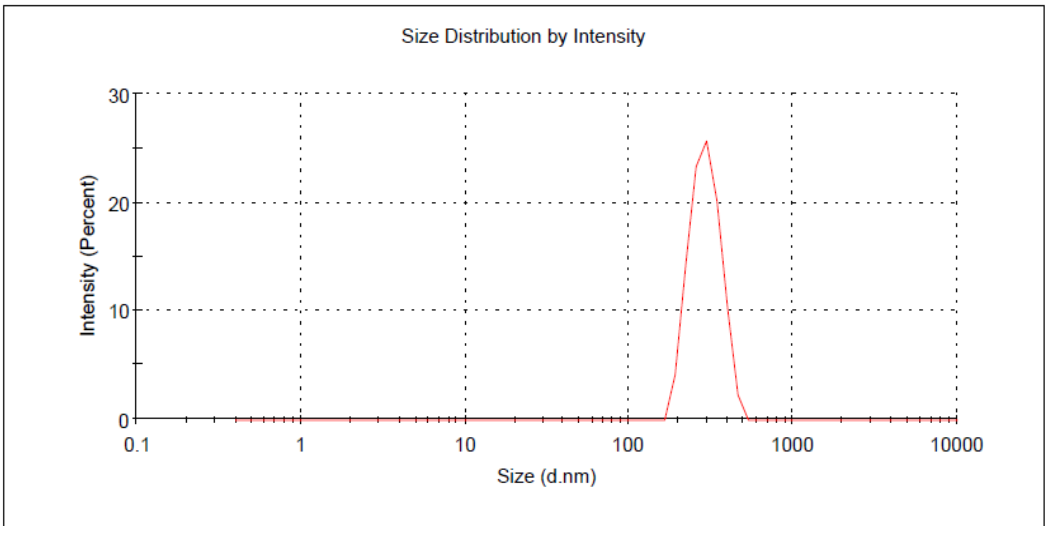

Fig. S1 DLS analysis of cNP and RBcNP.

Table S1. Antibodies used in flow cytometry analyses.

Antibody	Fluorochrome	Concentration	Internal/External	Supplier	Cat. Number
CD45	PE-Cy7	0.125µg/test	External	Thermo	25-0451-82
CD3	APC-eFluor780	1µg/test	External	Thermo	47-0032-82
CD4	Alexa Fluor 700	0.125µg/test	External	Thermo	56-0041-82
CD8a	PE	0.25µg/test	External	Thermo	12-0081-82
CD25	PE-Cy5	0.125µg/test	External	Thermo	15-0251-82
FoxP3	APC	1µg/test	Internal	Thermo	17-5773-82

Table S2. Flow cytometry gating strategy.

PBMCs	CD45	CD3	CD4	CD8a	CD25	FoxP3
T Helper	+	+	+	-	-	-
Cytotoxic	+	+	-	+	-	-
T_{Reg}	+	+	+	-	+	+

Toxicity of systemically administered nanoparticles

For liver tissues, histological examination revealed normal lobular architecture and no evidence of fibrosis (Fig.2SA left and B1,2)). Limited, non-specific, inflammatory cell aggregates were noted in both control and recipient animals. One case contained a small granuloma. As an isolated finding this was considered to be of limited significance. There was no evidence of steatosis and no significant differences between control and test liver samples (Fig.1SA left and B1, 2). For kidney sections, there was no cytoplasmic vacuolation within either proximal or distal tubules no evidence of acute tubular necrosis (Fig.1SA right and B3-6). 4 kidneys exhibited focal patchy chronic interstitial inflammation that was also present in control sections and was therefore deemed to be of little significance in the current context. There was no glomerular abnormality in samples that were exposed to the cNPs. The vessels were normal with several showing mild venous dilatation and again this was unlikely to be of any significance. The collecting system was normal in all kidneys. Some perinephric brown fat was observed. In summary, there were no significant pathological findings in either control or treated kidneys.

A

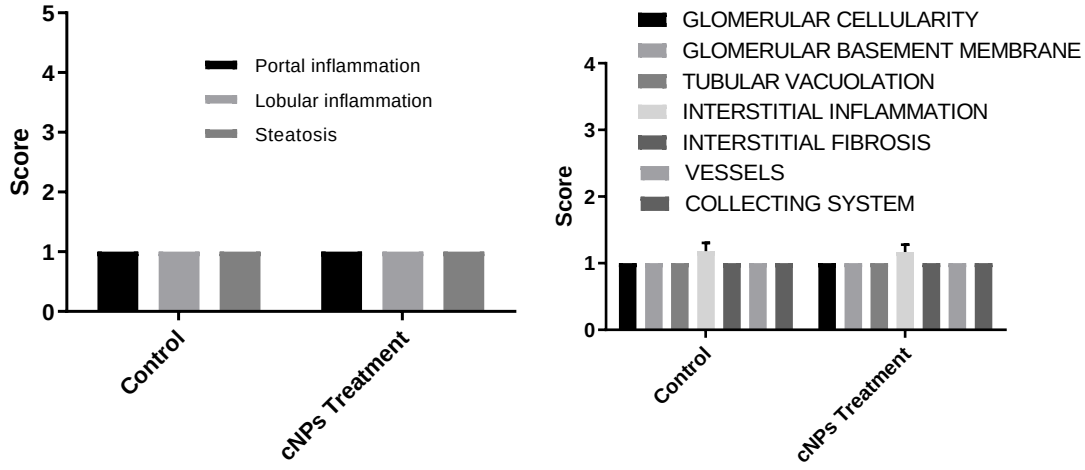

B

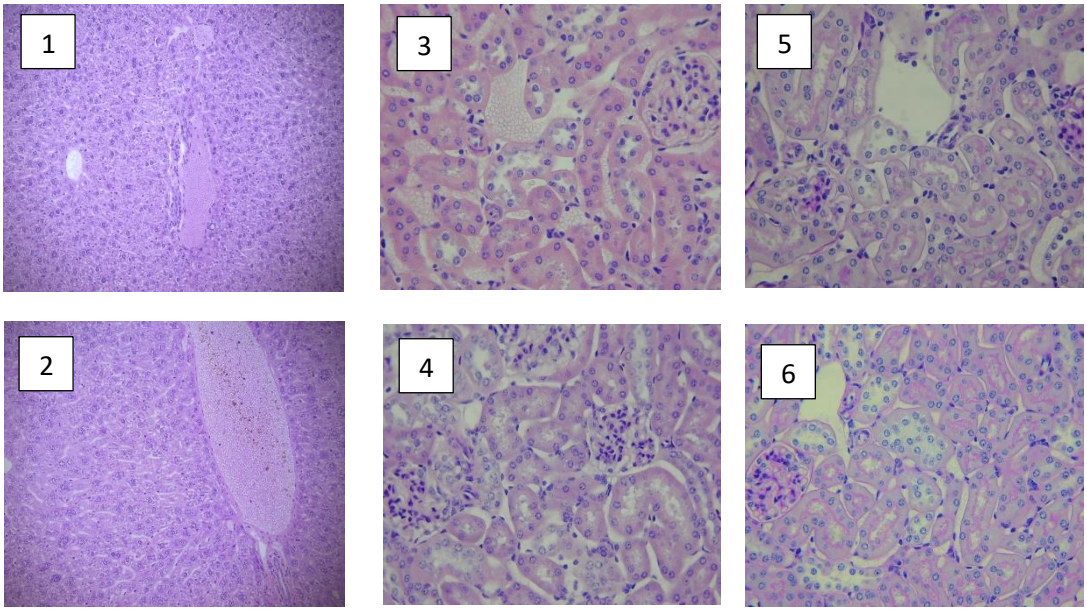

Liver = X20 **Kidney x 240**

Figure S2 (A) Histological analysis of liver (left) and kidney (right) harvested from CD-1 mice 7 days after IV administration of cNPs. Error bars represent ± SD and n = 12. (B) Photomicrographs of representative images from control (1) and cNP exposed (2) liver sections following H & E staining and control (3 and 5) and cNP exposed (4 and 6) kidney sections following H & E staining (3 & 4) and PASD staining (5 and 6).